Biosensors and Bioelectronics 130 (2019) 48–54

Contents lists available at ScienceDirect

Biosensors and Bioelectronics

journal homepage: www.elsevier.com/locate/bios

Comparison of enzymatic and non-enzymatic glucose sensors based on hierarchical Au-Ni alloy with conductive polymer

Won-Chul Lee[a], Kwang-Bok Kim[c], N.G. Gurudatt[a,d], Khalil K. Hussain[a], Cheol Soo Choi[d], Deog-Su Park[b,*], Yoon-Bo Shim[a,b,*]

[a] Department of Chemistry, Pusan National University, Busan 46241, South Korea
[b] Institute of BioPhysio Sensor Technology (IBST), Pusan National University, Busan 46241, South Korea
[c] Biomedical System & Technology Group, Korea Institute of Industrial Technology, Cheonan 31056, South Korea
[d] Endocrinology, Internal Medicine, Gil Medical Center, and Korea Mouse Metabolic Phenotyping Center, Lee Gil Ya Cancer and Diabetes Institute, Gachon University College of Medicine, Incheon 21999, South Korea

ARTICLE INFO

Keywords:
Hieratical Au-Ni alloy
Amperometric biosensor
Conducting polymer
Glucose sensor

ABSTRACT

Enzymatic and non-enzymatic amperometric glucose sensors based on nanostructured Au-Ni alloy were prepared and compared in their performance. The hierarchically structured Au-Ni surface was merely used for the non-enzymatic glucose sensor, while glucose oxidase attached poly-3′(benzoic acid) −2,2′:5′,2′- terthiophene (pTBA) formed on the alloy surface was used as the enzymatic sensor. The fabricated sensor was characterized using surface analysis and electrochemical experiments. In case of the enzymatic sensor, the anodic current of H_2O_2 generated from the enzyme reaction was used as the analytical signal, while the direct oxidation of glucose was observed on a mere Au-Ni alloy electrode without enzyme immobilization, which shows an excellent catalytic oxidation of glucose even in physiological pH. The potential pulse pretreatment of the sensor surfaces improved the performance, which allowed both the sensors reproducible and reusable (enzymatic sensor: coefficient of variation = 1.82%, n = 5, non-enzymatic: coefficient of variation = 2.93%). The enzymatic biosensor reveals the advantages of increased sensitivity, selectivity, and stability, compared with the non-enzymatic sensor. The linear range of enzymatic sensor was attained from 1.0 μM to 30.0 mM with a detection limit of 0.29 μM. The reliabilities of the sensors were also demonstrated through the glucose analysis in human blood samples, and the result was compared with the commercially available glucometer.

1. Introduction

Diabetes mellitus is one of metabolic disease concerned with fluctuation in blood sugar level that might result in a serious damage to various body systems, such as cardiovascular, urinary, and nervous (Association, 2014). Despite the lack of any known cure for diabetes, frequent monitoring of blood glucose levels is crucial for understanding diabetes progression toward optimal management of the disease. Therefore, it is essential to develop a sensitive detection system for clinical and biomedical applications (Beck et al., 2008).

Several methods for glucose analysis have been reported to date, including high-performance liquid chromatography (HPLC) (Taguchi et al., 2003), capillary zone electrophoresis (Wang et al., 2016), optical (Sun et al., 2018), Fourier transform (FT) spectroscopy (Petibois et al., 1999), and other methods. Despite these methods have numerous advantages, they are expensive, require additional purification steps, trained personnel, and furthermore they cannot be converted to point of care devices. Therefore, the alternative sensitive and selective detection system using electrochemical methods is highly desirable, which are robust and capable of miniaturization for medical diagnosis (Zhang et al., 2008; Moon et al., 2018). Of these, many glucose sensors using electrochemical methods have been reported (Wang, 2008; Kim et al., 2013), which are mostly enzyme-based sensors and some of them are enzyme-free. Although, the great success in glucose sensor have been achieved so far, these sensor/biosensor still a challenging area of research. For example, the enzyme based sensors are usually somewhat expensive and unstable, and their catalytic activity is affected by several factors such as temperature, pH, and ionic strength (Wang, 2008). For this reasons, the non-enzymatic method has attracted attention in recent years, because of its low cost, rapid response, and exceptional sensitivity in some cases (Toghill and Compton, 2010). The sensing electrodes based on these materials, however, still have drawbacks such

* Corresponding authors.
E-mail addresses: dsupark@pusan.ac.kr (D.-S. Park), ybshim@pusan.ac.kr (Y.-B. Shim).

https://doi.org/10.1016/j.bios.2019.01.028
Received 20 November 2018; Received in revised form 29 December 2018; Accepted 7 January 2019
Available online 21 January 2019
0956-5663/

as poor stability, easy loss of activity, and surface poisoning from the adsorbed intermediates, especially low sensitivity at neutral pH.

In case of non-enzymatic sensor, metal or metal oxides have been mostly used as catalytic electrode materials (Hwang et al., 2018). In some cases, to enhance the catalytic properties of metallic nanoparticle, bimetal alloy was used as electrode materials, which are usually synthesized using elements in fully filled d-orbitals and the other metal atoms that have vacant d-orbitals (Jiao et al., 2015). Especially, they exhibit often better catalytic activities than the corresponding monometallic counterparts due to the synergistic effect, and it is also possible to additionally enhance their catalytic properties through shape and morphology control (Liu et al., 2012). The formation of hierarchical structure is one of ways to get the additional catalytic property that plays an important role for both the enzymatic and non-enzymatic sensor probes, because of its porous structure having higher surface area and pronounced surface reaction activity (Guo and Wang, 2011). Some of bimetal catalysts including novel metal (Shim et al., 2019) and transition metal (Noh et al., 2012b) nanoparticles have been reported as sensitive non-enzymatic sensors. We have recently observed that hierarchical Au-Ni bimetal alloy reveals a large catalytic activity for glucose oxidation even in neutral pH conditions, hence, it have been tried to compare the performance of enzymatic and non-enzymatic glucose sensors prepared with this catalytic material in physiological pH.

The most important step to fabricate a stable enzymatic biosensor is fixing enzymes without losing their stability or biological functions. One of the way is using the conducting polymer (CPs) composite, where the substrate polymer plays a significant role in the design of electrochemical biosensors (Rahman et al., 2008; Naveen et al., 2017; Kim et al., 2019). CPs are class of organic molecules and emerged as an essential element in the fabrication of sensors. Of these, polyterthiophene-based CPs are comparatively more stable than polyaniline (Shim et al., 1990) and polypyrrole (Park et al., 1993). In addition, polyterthiophene is low toxic, and a substrate having functional groups such as -NH_2 (amine) and/or -COOH (carboxylic acid) allows firm immobilization of biomolecules through the peptide bond formation between the polymer layer and the biomolecules (Ban et al., 2004; Noh et al., 2012a; Kim et al., 2013). Hence, we prepared the enzymatic sensor using a conducting polymer formed on hierarchically structured Au-Ni alloy to stably immobilize the GOx on the sensor probe.

In the present study, a hierarchically structured bimetal was demonstrated for enzymatic and non-enzymatic glucose sensors in human whole blood and their performances were compared each other. The mere hierarchical Au-Ni alloy was used as a non-enzyme sensor probe for the detection of glucose at the physiological pH. The enzymatic sensor was fabricated by covalent bonding of glucose oxidase (GOx) on a benzoic acid bearing conducting polymer formed on the same alloy layer. Fabrication and characterization of each sensor layer were demonstrated using electrochemical and surface characterization techniques. The analytical signals were monitored via the direct oxidation of glucose for the non-enzymatic sensor or the catalytic oxidation of H_2O_2 generated from the enzymatic reactions on the sensor surface. Various parameters affecting the sensor probe were optimized and the reliability of the sensor was investigated by detecting glucose in real samples, where the results were compared with a commercially available glucometer.

2. Experimental

2.1. Fabrication of the sensor probe

The details of chemicals and instruments are described in Supplementary information. The sensor was fabricated as shown in Scheme 1. Firstly, the hierarchical Au-Ni alloy was electrochemically formed on SPCE (screen-printed carbon electrode) with a 0.1 M Na_2SO_4 solution containing 30.0 mM $HAuCl_4{\cdot}4H_2O$ and 15.0 mM $NiSO_4$ employing chronoamperometry at −0.8 V for 200 s. In case of the non-enzymatic sensor, glucose molecules were oxidized to a final product of gluconolactone at the surface of metal hydroxides formed during the anodic scan. On the other hand, metal ions formed at glucose oxidation potential will have a subsequent reduction in the presence of oxygen as shown in Scheme 1. The final nonenzymatic sensor was coated with 0.5% Nafion (NF) by drop casting. Otherwise, the enzymatic sensor was prepared through electrochemical polymerization of pTBA on the Au-Ni layer with three potential cycling from 0.0 to 1.1 V (Ag/AgCl) at 0.1 V/s in 0.1 M PBS (pH 7.4). The pTBA/Au-Ni electrode was immersed in 10.0 mM EDC and NHS containing 0.1 M PBS (pH 7.4) for 3 h to activate the carboxylic acid groups on the pTBA layer. Then, the electrode was washed twice with double distilled water and subsequently incubated in 6.0 mg/ml FAD-glucose oxidase (GOx) containing 0.1 M PBS (pH7.4) for 3 h. Finally, 0.5 μL of 0.5% Nafion (NF) was drop casted onto the final enzymatic sensor layer and dried at room temperature for the analysis of glucose monitoring.

2.2. Analytical procedure

The non-enzymatic glucose sensor was tested for its performance in 0.1 M PBS (pH7.4) for the direct electrochemical oxidation of glucose, whereas the glucose detection using the enzymatic sensor was performed in 0.1 M PBS (pH 7.4) solution and the normal person whole blood samples (five volunteers). The most enzymatic glucose sensor were based on monitoring the anodic current of H_2O_2 produced by the enzyme reaction. The ampermetric responses for the non-enzymatic and the enzymatic sensors were obtained at the applied potential of + 0.05 V and + 0.40 V (vs. Ag/AgCl), respectively for various glucose concentrations (non-enzymatic: 10.0 μM–20.0 mM; enzymatic: 1.0 μM–30.0 mM) in 0.1 M PBS (pH 7.4). In case of human whole blood samples, the result was compared with the comparative method using a commercial glucose meter (One Touch UltraTM, Lifescan Inc.).

3. Results and discussion

3.1. Morphology and surface characteristics of Au-Ni bimetal

The surface morphology of the Au-Ni bimetal layer was studied using XRD, FE-SEM and HR-TEM. The XRD analysis was performed for Au-Ni alloy (Fig. 1(A)), which shows the typical Au and Ni peaks at 2θ values of Au (38.18°, 44.39°, 64.58°, 77.56°, 81.72°) and Ni (39.1°, 44.5°, 78.0°, 84.1°), respectively. The index peaks, assigned as Au ((111), (200), (220), (311), and (222)) and Ni ((010), (011), (110), and (103)), identify the material as fcc (Au and Ni) phase. All the peaks for Au and Ni were assigned to the cubic phases of metallic Au (JCPDS 04-0784) and Ni (JCPDS 45-1027), respectively. The X-RD pattern of Au-Ni in high intensity corresponding to Au and Ni are homogeneously dispersed. Overall, the homogeneous distributions of Au and Ni in the nanostructures are expected to enhance the catalytic oxidation of H_2O_2.

The FE-SEM image (Fig. 1(B)) reveals as-prepared heiratical structure in the nanoscale range, where its large surface area can result in the enhancement of both the catalytic effect toward hydrogen peroxide and glucose oxidation reactions. Otherwise, the pTBA coated Au-Ni layer shows a reduced pore size of the structure (Fig. S1(A)). After GOx was bonded on pTBA/Au-Ni layer, it does not clearly show nanostructure but displays a very rough enzyme surface (Fig. S1(B)). Furthermore, Fig. S1(C) shows the EDXS data for the Au-Ni alloy layer. Both the elements of Au-Ni were detected and wt% contents of Au and Ni were 62.59% and 37.41%, respectively. The HR-TEM image confirmed the crystalline structure of Au-Ni alloy. As shown in Fig. 1(C), the Au-Ni alloy forms well-defined lattice spacing of 0.235 nm and 0.203 nm matched with the Au (111) and Ni (011) planes, respectively. Inset of Fig. 1(C) shows the selected-area electron diffraction (SAED) pattern, exhibiting the mixed diffraction rings of fcc-Au and fcc-Ni. This indicates the formation of hierarchical nanostructure with intermixing of each element. The corresponding SAED pattern is consistent with the

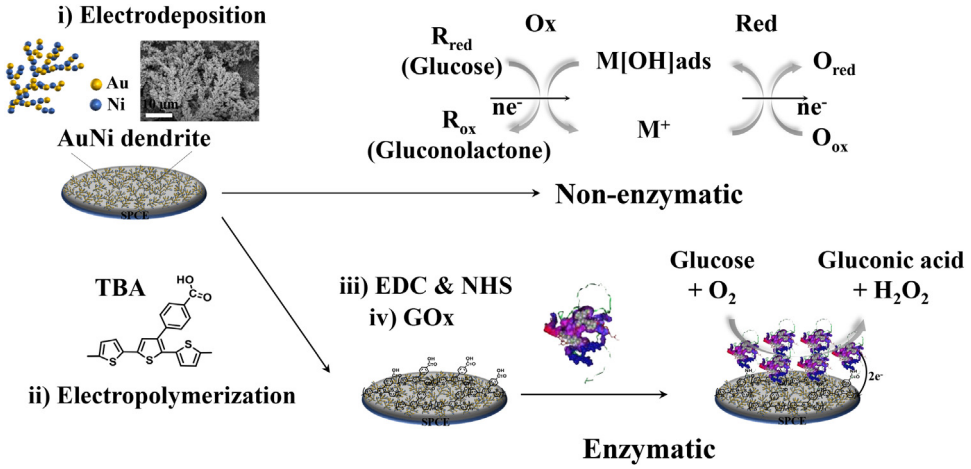

Scheme 1. Schematic representation of the sensors fabrication and detection mechanism.

XRD result. The content ratios of the Au-Ni alloy was determined to do the elemental mapping of Au and Ni as shown in Fig. 1(D(i-iv)). The mapping data for Au and Ni atoms confirm the formation of Au-Ni. The merged mapping data shows clear evidence for the elemental distribution in the alloy structure. These results obtained in FE-SEM and HR-TEM images confirm the formation of hierarchical Au-Ni alloy layer.

3.2. Immobilization of the sensing layer

To demonstrate the chemical binding between polymer and immobilizing enzyme, XPS analysis was carried out, where the spectra were obtained for Au4f, Ni2p, C1s, N1s, and S2p as shown in Fig. 2. The survey spectra of GOx-pTBA/Au-Ni layer show the presence of Au4f, S2p, C1s, N1s, O1s, and Ni2p peaks in Fig. 2(A). Further, the deconvoluted spectra of (B) Au4f, (C) Ni2p, (D) C1s, (E) Au4f, and (F) S2p were obtained for (i) Au-Ni, (ii) pTBA/Au-Ni, and (iii) GOx-pTBA/Au-Ni. The Au4f spectrum of Au-Ni layer (i) reveals typical two peaks at 83.2 ($Au4f_{5/2}$) and 86.8 ($Au4f_{7/2}$) eV. Otherwise, the binding energy is shifted to the lower value (0.23 eV) after electropolymerization of TBA monomer on Au-Ni (ii) (Fig. 2(B)). Fig. 2(C(i-ii)) shows the metallic Ni formation, where the prominent peaks for Ni oxide and $Ni(OH)_2$ reveal

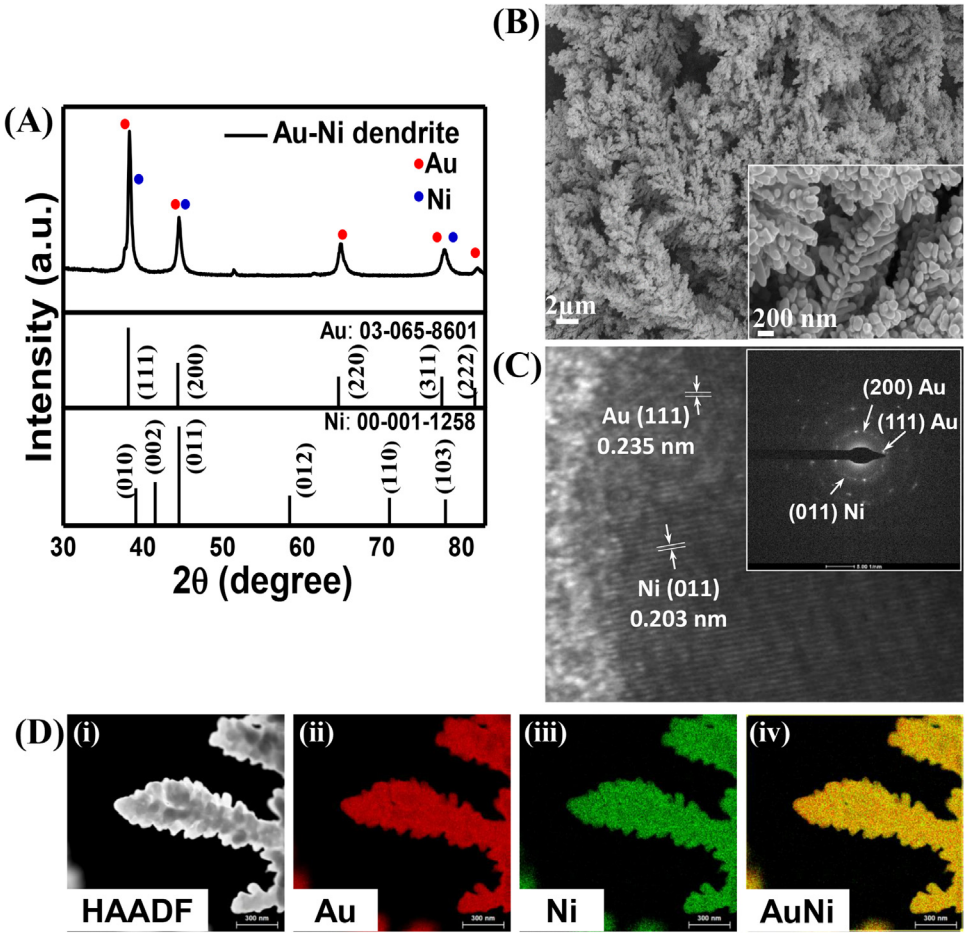

Fig. 1. (A) XRD spectra of Au-Ni alloy. (B) FE-SEM images of Au-Ni alloy (Inset: The magnified FE-SEM image). (C) HR-TEM high magnified section image of Au-Ni (inset: corresponding SAED patterns for sample). (D-i) High-angle annular dark-field scanning transmission electronmicroscopy (HAADF-STEM), (D-(ii-iv)) elemental mapping of Au-Ni alloy.

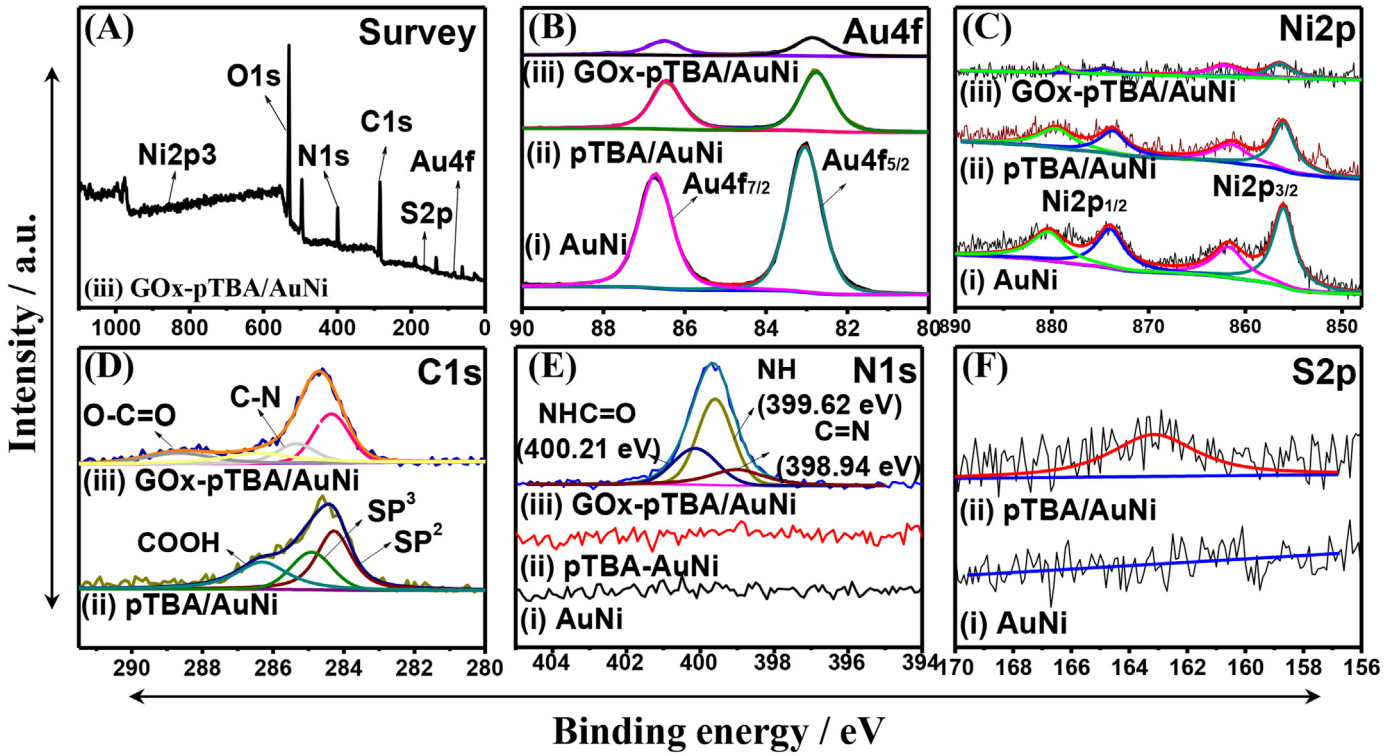

Fig. 2. XPS spectra of (A) survey, (B) Au4f, (C) Ni2p, (D) C1s, (E) N1s, and (F) S2p peaks for (i) Au-Ni, (ii) pTBA/Au-Ni and (iii) GOx-pTBA/Au-Ni.

at 861.6 and 879.2 eV, respectively (Yan et al., 2012), and the content of Ni oxide is high than that of Au, which owe to the higher affinity of Ni to oxygen than Au. The intensity of the Ni peaks in the spectra of the pTBA/Au-Ni (ii) and GOx-pTBA/Au-Ni (iii) decreased as compared to the Au-Ni layer due to the polymer layer and immobilized enzyme. In the case of C1s spectra, after electropolymerization of TBA on Au-Ni (ii), the peak at 286.23 eV (-COOH of TBA) was appeared. After immobilization of GOx (iii), the O-C=O peak from GOx component and the N-C peak indicating the formation of covalent bond between pTBA and GOx are newly observed at 288.87 eV and 285.42 as shown in Fig. 2(D). In this case, the -COOH peak is slightly shifted to higher energy at 287.74 eV. The N1s spectrum of GOx-pTBA/Au-Ni (iii) reveals three new peaks for GOx at 400.21 (HNC=O), 399.62 (NH), and 398.94 eV (C=N) (Fig. 2(E)). The S2p spectrum shows a peak at 163.2 eV, corresponding to the presence of S in the terthiophene backbone of pTBA (Fig. 2(F)). The results additionally confirmed the immobilization of GOx onto the pTBA layer.

3.3. Electrochemical properties of the sensor probe

In case of bimetallic alloy materials, including gold, nickel, and cobalt etc., the glucose oxidation process is dominant in alkaline solution than in neutral one (Miao et al., 2014). However, the hierarchical Au-Ni surface shows an excellent performance for direct glucose oxidation in 0.1 M PBS (pH 7.4) as shown in Fig. 3(A). The CV recorded for the electrode shows the direct oxidation of glucose around + 0.02 V, where the peak current increased by increasing glucose concentrations from 0.1 to 10.0 mM. On the other hands, the Au-Ni electrode also reveals the catalytic oxidation reaction of H_2O_2 in PBS solution; In the CV, the oxidation peak of H_2O_2 was observed at + 0.34 V as shown in Fig. 3(B). As the concentration of H_2O_2 increased from 0.01 to 1.0 mM, the peak current increased. Further, the GOx-pTBA/Au-Ni probe as an enzymatic glucose sensor was examined to detect the enzymatically generated H_2O_2 in the glucose solution as shown in Fig. 3(C). The anodic peak current corresponding to the oxidation of H_2O_2 increased linearly by increasing the glucose concentration from 0.01 to 10.0 mM, indicating a stable conversion of glucose by enzyme reaction. It is worth to note that there is no difference in the oxidation potential for both the standard H_2O_2 solution and enzymatically generated H_2O_2. These results confirm that the GOx immobilized hierarchical Au-Ni sensor probe is capable of sensitive detection of glucose through the monitoring the H_2O_2 generated by the enzyme reaction.

The electrochemical impedance spectroscopy (EIS) was measured to investigate the electrical characteristic of each layer in a 0.1 M PBS (pH 7.4) solution. Fig. 3(D) shows Nyquist plots obtained for (i) SPCE, (ii) Au-Ni/SPCE, (iii) pTBA/Au-Ni/SPCE, (iv) GOx-pTBA/Au-Ni/SPCE, and the data for corresponding layers were fitted based on a Randle circuit (inset of Fig. 3(D)). The R_{CT} (Rp2 + Rp3) were determined employing Zview 2 impedance software, where the R_{CT} value for bare SPCE was calculated to be 39.2 kΩ, while Au-Ni on the SPCE lowered the R_{CT} value to 8.5 kΩ, which was about 4.6 times lower than that of the SPCE. This indicates that the Au-Ni cause the conductivity increase. After the formation of pTBA polymer layer, the charge transfer resistance increased to 13.7 kΩ. Furthermore, the R_{CT} values of GOx-pTBA/Au-Ni increased to 19.7 kΩ due to somewhat impeding of the electron-transfer by GOx immobilization on the polymer layer.

3.4. Optimization of experimental parameters

The experimental parameters for the glucose detection with both the sensors were optimized, in terms of Au-Ni concentration ratio, deposition time and potential of Au-Ni alloy, temperature, amount of GOx, pH, and detection potentials in a 0.1 M PBS (pH7.4) containing 1.0 mM glucose solution as shown in Fig. S2. As shown in Fig. S2(A), the highest oxidation current was observed in the ratio of 30:15 for Au:Ni, respectively. As the deposition potential for the metal alloy changed from −0.5 V to −0.8 V, a gradual increase in the current response for the glucose oxidation was observed. When the potential increased beyond −0.8 V, a sharp current decrease was observed as shown in Fig. S2(B). Hence, −0.8 V was chosen as the optimum deposition potential. Similarly, the deposition time was changed from 100 to 1000 s to optimize the metal alloy formation as shown in Fig. S2(C).

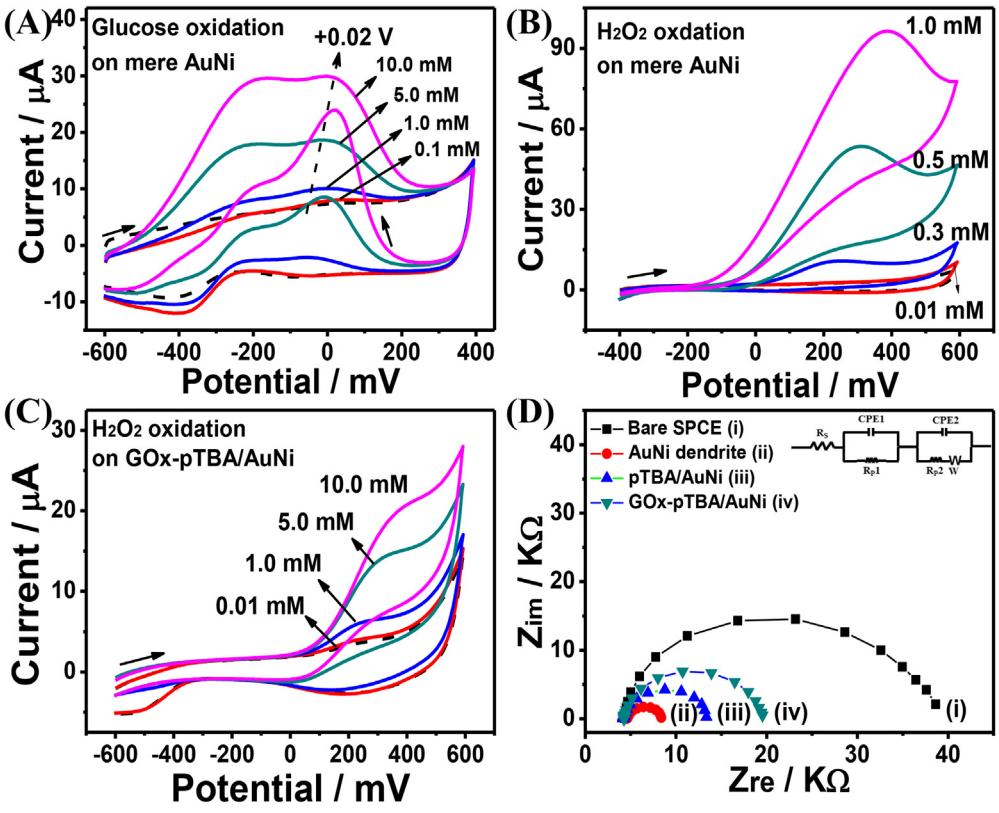

Fig. 3. CVs recoded for mere Au-Ni/SPCE in various concentration of (A) glucose (0.1–10.0 mM) and (B) H_2O_2 (0.01–1.0 mM), (0.1 M PBS, dashed line). (C) CVs recoded for GOx-pTBA/Au-Ni/SPCE (enzymatic) in different concentrations of glucose (0.01–10.0 mM), (0.1 M PBS, dashed line). (D) Nyquist plots obtained for (i) bare SPCE, (ii) Au-Ni/SPCE, (iii) pTBA/Au-Ni/SPCE, and (iv) GOx-pTBA/Au-Ni/SPCE in a 0.1 M PBS (pH 7.4) solution.

The response current increased from 100 s to 200 s and maintained a constant over 200 s, followed by a decrease due to the saturation of the electrode surface. Fig. S2(D) shows the loaded enzyme amount, the anodic response increased gradually as the amounts of glucose oxidase increased from 3.0 to 6.0 mg/ml and reached a steady state at greater than 6.0 mg/ml GOx. Therefore, 6.0 mg/ml GOx was used to immobilize the sensor probe in the subsequent experiments. The pH was changed between 5.5 and 8.0, where the response gradually increased as the from 5.5 to 7.4. The maximum response was obtained at pH 7.4 (Fig. S2(E)), which is the physiological pH of blood. Temperature was controlled between 10 and 60 °C, and the maximum signal was measured at 45 °C, and then it decreased over 50 °C due to the instability of the sensor surface over 50 °C (Fig. S2(F)). Although the maximum response was observed at 45 °C, we selected 25 °C as the measurement temperature, because real samples are usually measured at room temperature. In case of the non-enzymatic sensor, the detection potential for the direct oxidation of glucose was studied. The response increased from −0.05 V to + 0.05 V, then saturated from + 0.10 V. Hence, the detection potential optimized at + 0.05 V (Fig. S2(G)). Furthermore, the H_2O_2 oxidation response for the enzymatic sensor was studied from + 0.10 to + 0.50 V. The anodic response increased as the detection potential increased from + 0.10 V, the maximum response was obtained at + 0.40 V (Fig. S2(H)). Hence, the + 0.40 V was used for the final analysis.

3.5. Performance comparison of enzymatic and non-enzymatic sensors

Under the optimized conditions, the performances of both the sensors were compared in terms of their sensitivity, selectivity, and stability towards glucose detection in whole blood. The amperograms obtained for the enzymatic sensor (Fig. 4(A), solid line) show a dynamic range between 1.0 μM and 30.0 mM. Otherwise, the non-enzymatic sensor showed a narrower dynamic range from 10 μM to 20 mM as shown in Fig. 4(A) (short dashed line). Further, compared to single metal such as, Au and Ni, the Au-Ni alloy revealed higher response to glucose oxidation due to the synergetic effect of two metals as shown in the CV (Fig. S3). The calibration plots obtained for both the sensors show that the current response increased linearly to the concentration of glucose. The sensitivity of the enzymatic sensor calculated from the

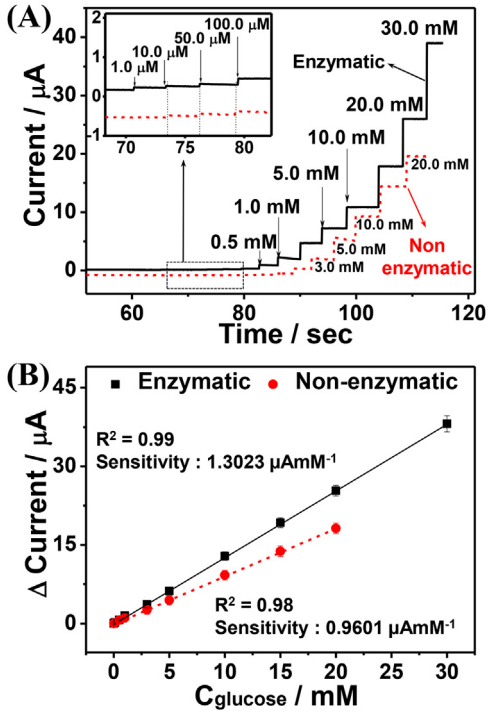

Fig. 4. (A) Amperometric responses for glucose detection using enzymatic (solid line) and nonenzymatic sensors (dotted line). (Inset reveals the current response at low glucose concentrations). (B) Calibration plots of both the sensors obtained by successive addition of glucose in 0.1 M PBS (pH 7.4) solution.

calibration plot in Fig. 4(B) (solid line) is 1.30 μA/mM with the detection limit of 0.29 μM. The calibration plot shows an excellent linearity to the glucose concentration with 0.99 coefficient of variation (R^2). Similarly, the non-enzymatic sensor (short dashed line) shows a sensitivity of 0.96 μA/mM with a detection limit of 5.84 μM and an R^2 value of 0.98. The results clearly show the superior analytical performances in sensitivity, linear range, detection limit, and repeatability when the sensor probe was enzymatically fabricated. It might be resulted from the catalytic activity of Au-Ni dendritic nanostructure to H_2O_2 oxidation is more higher than that of glucose. Table S1 shows a comparison of proposed enzymatic and non-enzymatic glucose sensor performances with other bimetallic glucose sensors. As compared to other electrode materials, proposed sensor probe materials have excellent sensitivity and low detection limit.

3.6. Interference effects and long-term stability

To improve the reproducibility and reusability of the sensors, we pretreated the sensor probe by applying the potential pulse between −0.4 V and + 0.6 V prior to each measurement. When both the sensors were pretreated, it was found that the pretreatment allowed them for a more reproducible response as shown in Fig. 5(A). After pretreatment, the disposable sensors exhibited excellent reproducible responses towards glucose (0.1 mM glucose in PBS (pH 7.4)) oxidation for five times repeated measurements, with coefficient of variation of 1.82% and 2.93% (n = 5) for enzymatic and non-enzymatic methods, respectively. Otherwise, untreated sensors showed low coefficient of variation values (enzymatic = 12.7%, non-enzymatic = 37.5%, n = 5), indicating that electrodes with step pulse method displayed highly stable and reproducible performance. Hence, all the experiments to detect glucose were conducted with the pretreatment before using them.

The sensors were evaluated for their selectivity towards a glucose standard solution in the presence of different interference species, such as uric acid (UA), ascorbic acid (AA), dopamine (DP), and acetaminophen (AP). All interference test samples were prepared using 0.1 M in PBS (pH 7.4). The electrochemical oxidation reactions of these biomolecules were observed in the same potential window to the glucose detection. The current response of the enzymatic sensor (solid line) was recoded at + 0.4 V in the PBS solution containing the foreign species as shown in Fig. 5(B). The concentrations of interference species added in the measuring solution were 0.1 mM of dopamine (DA), acetaminophen (AP), ascorbic acid (AA), and uric acid (UA). The results show that the interference effect of each species was 1.5% to AA, 2.8% to AP, 1.9% to UA, and 2.5% to DA. However, in case of non-enzymatic sensor (short dashed line), when glucose was introduced into the solution containing interference species, the noticeable variation in response was observed. The long-term stability of both the proposed enzymatic (solid line) and non-enzymatic (short dashed line) sensors were examined a time per day for 30 and 18 days, respectively (Fig. 5(C)). In case of the enzymatic sensor, 95.3% of its initial response was retained after 30 days. This indicates that the proposed enzymatic sensor possesses good stability, which is owe to the strong chemical binding of the enzyme onto the stable conducting polymer layer. Otherwise, the non-enzymatic sensor showed that 60.4% of initial response retained after 18 days.

3.7. Real sample analysis

The reliabilities of bothe the enzymatic and non-enzymatic sensors were evaluated by determining the glucose concentration in finger pricked human blood samples obtained from healthy volunteers (n = 5). The real sample measurements were performed. The results from three times measurements for each sample were compared with that from the commercial glucose monitoring meter (One Touch Ultra, Lifescan lnc.) as shown in Table S2. The data were evaluated by the paired *t*-test, and the calculated t values (enzymatic: 0.28, non-enzymatic: 1.39) were less than the critical t value (< 1.76) at the 95% confidence level (n = 5). The enzymatic glucose sensor showed an excellent agreement with the commercial glucose meter, while somewhat irreproducible result was obtained for the non-enzymatic sensor.

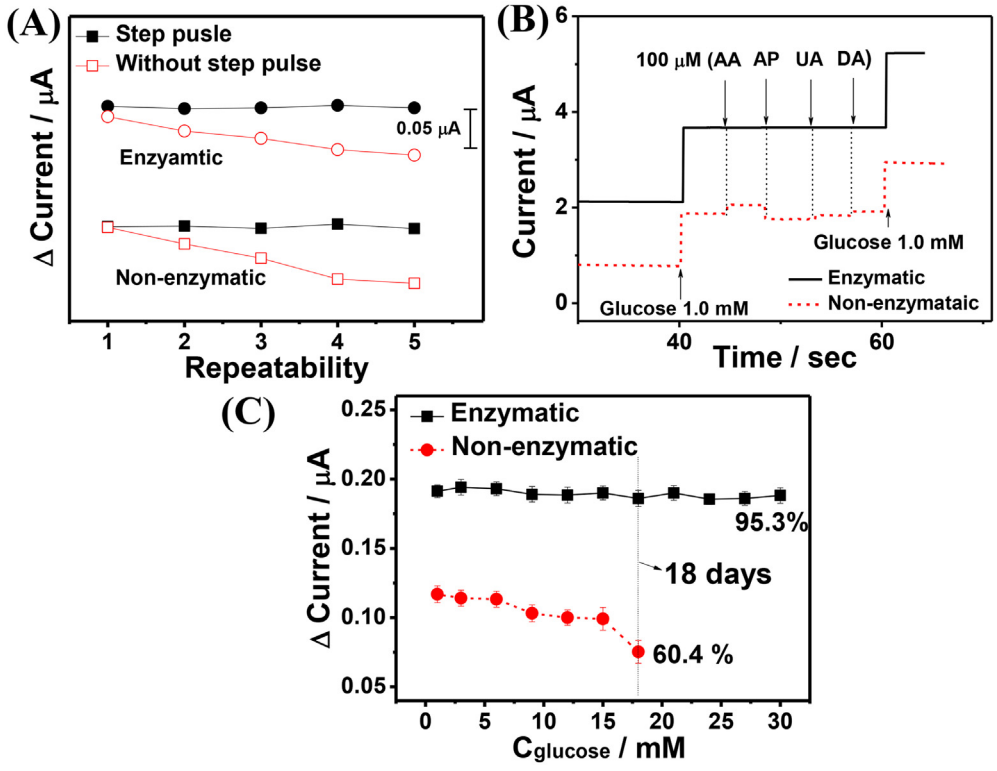

Fig. 5. (A) Repeatability and reusability of enzymatic and non-enzymatic sensors (in 0.1 mM glucose solution) with and without potential pulse pretreatment. (B) Amperometric response of both the glucose sensors in the presence of interfering species. (C) Long-term stability of the both glucose sensors in 0.1 mM glucose solution, respectively.

4. Conclusions

Enzymatic and non-enzymatic glucose sensors were prepared using nanostructured Au-Ni alloy as a substrate electrode and their performances were compared. The results revealed the superior analytical performance of the enzymatic sensor, where the sensitivity was 1.4 times higher and detection limit was 20.1 times lower compared with non-enzymatic one. Further, the enzymatic sensor showed an excellent selectivity, stability, and linear range, which was due to the stable enzyme immobilization onto the pTBA surface. Finally, the reliability of the proposed sensors was evaluated using finger pricked blood samples, where they showed good agreement with the result of the commercially available glucose meter. The significance of this work is directly related to the various fields, such as clinical, pharmaceutical, and biomedical applications.

Acknowledgements

This work was partially supported by a grant from the Korea Health Technology R&D Project through KHIDI funded by the Ministry for Health and Welfare of Korea (HI14C1135 & HI15C0987), and by the Philosys Co., Ltd.

Declaration of interests

None.

Appendix A. Supporting information

Supplementary data associated with this article can be found in the online version at https://doi.org/10.1016/j.bios.2019.01.028.

References

Association, A.D., 2014. Diagnosis and classification of diabetes mellitus. Diabetes Care 37, S81–S90.
Ban, C., Chung, S., Park, D.S., Shim, Y.B., 2004. Nucleic Acids Res. 32, 110.
Beck, W.V., Bode, B.W., Buckingham, B., Chase, H.P., Clemons, R., Fiallo-Scharer, R., Fox, L.A., Gilliam, L.K., Hirsch, I.B., 2008. N. Engl. J. Med. 359, 1464–1476.
Guo, S., Wang, E., 2011. Nano Today 6, 240–264.
Hwang, D.W., Lee, S., Seo, M.J., Chung, T.D., 2018. Anal. Chim. Acta 1033, 1–34.
Jiao, Y., Zheng, Y., Jaroniec, M., Qiao, S.Z., 2015. Chem. Soc. Rev. 44, 2060–2086.
Kim, D.-M., Kim, M.-Y., Reddy, S.S., Cho, J.G., Cho, C.-H., Jung, S., Shim, Y.-B., 2013. Anal. Chem. 85, 11643–11649.
Kim, K.-B., Lee, W.-C., Cho, C.-H., Park, D.-S., Cho, S.J., Shim, Y.-B., 2019. Sens. Actuators B-Chem. 281, 14–21.
Liu, X., Wang, D., Li, Y., 2012. Nano Today 7, 448–466.
Miao, Y., Ouyang, L., Zhou, S., Xu, L., Yang, Z., Xiao, M., Ouyang, R., 2014. Biosens. Bioelectron. 53, 428–439.
Moon, J.-M., Thapliyal, N., Hussain, K.K., Goyal, R.N., Shim, Y.-B., 2018. Biosens. Bioelectron. 102, 540–552.
Naveen, M.H., Gurudatt, N.G., Shim, Y.-B., 2017. Appl. Mater. Today 9, 419–433.
Noh, H.-B., Chandra, P., Moon, J.O., Shim, Y.-B., 2012a. Biomaterials 33, 2600–2607.
Noh, H.-B., Lee, K.-S., Chandra, P., Won, M.-S., Shim, Y.-B., 2012b. Electrochim. Acta 61, 36–43.
Park, D.-S., Shim, Y.-B., Park, S.-M., 1993. J. Electrochem. Soc. 140, 609–614.
Petibois, C., Rigalleau, V., Melin, A.M., Perromat, A., Cazorla, G., Gin, H., Déléris, G., 1999. Clin. Chem. 45, 1530–1535.
Rahman, M.A., Kumar, P., Park, D.-S., Shim, Y.-B., 2008. Sensors 8, 118–141.
Shim, K., Lee, W.-C., Park, M.-S., Shahabuddin, M., Yamauchi, Y., Hossaina, M.S.A., Kim, J.H., 2019. Sens. Actuators B-Chem. 278, 88–96.
Shim, Y.-B., Won, M.-S., Park, S.-M., 1990. J. Electrochem. Soc. 137, 538–544.
Sun, K., Yang, Y., Zhou, H., Yin, S., Qin, W., Yu, J., Chiu, D.T., Yuan, Z., Zhang, X., Wu, C., 2018. ACS Nano 12, 5176–5184.
Taguchi, T., Miwa, I., Mizutani, T., Nakajima, H., Fukumura, Y., Kobayashi, I., Yabuuchi, M., 2003. Clin. Chem. 49, 181–183.
Toghill, K.E., Compton, R.G., 2010. Int. J. Electrochem. Sci. 5, 1246–1301.
Wang, J., 2008. Chem. Rev. 108, 814–825.
Wang, X., Ma, Y., Zhao, M., Zhou, M., Xiao, Y., Sun, Z., Tong, L., 2016. J. Chromatogr. A 1469, 128–134.
Yan, J., Sun, W., Wei, T., Zhang, Q., Fan, Z.J., Wei, F., 2012. J. Mater. Chem. 22, 11494.
Zhang, X.J., Ju, H.X., Wang, J., 2008. Electrochemical Sensors, Biosensors and Their Biomedical Applications. Elsevier, New York.